Bandgap Pairing in Three-Terminal Tandem Solar Cells: From Limiting Efficiency to Voltage-Matched Device Performance

Philipp Wagner, Philipp Tockhorn, Lea Zimmermann, Eike Köhnen, Silvia Mariotti, Florian Scheler, Marlene Härtel, Steve Albrecht, and Lars Korte**

Three-terminal tandem solar cells (3 T TSCs) have recently sparked increasing interest as they feature a lean monolithic device architecture similar to two-terminal TSCs and, like four-terminal TSCs, do not require current matching for optimal operation. In this contribution, detailed balance limit calculations for different combinations of top and bottom cell bandgaps are conducted to determine the optimum bandgap pairing and limiting efficiency of 3T TSCs. An experimental realization of a 3T TSC with perovskite and silicon sub-cells and a combined efficiency of 28.9% is presented and used to derive a realistic parameterization for non-radiative recombination. Herein, the optimum bandgap pairing and resulting maximum efficiency under voltage-matched conditions for voltage-matching ratios of 1:2 and 2:3, which is relevant for stringing and module integration of 3T TSCs, are further determined. To this end, non-radiative recombination is incorporated in the model and quantified by matching theoretical open-circuit voltages and those of real-world high-efficiency solar cells based on different absorber materials (and thus bandgaps), including the perovskite top cell of the best in-house 3T TSC.

1. Introduction

The concept of detailed balance was introduced by Shockley and Queisser in 1961 to establish a thermodynamic efficiency limit of solar cells with a single-bandgap absorber.[1] It is based upon the assumption that absorption and emission of radiation must be equal, with solar cell and sun each being ideal blackbodies at temperatures of 300 and 6000 K, respectively. For such a device, the optimal bandgap lies at 1.1 eV, and the maximum attainable power conversion efficiency (PCE) is slightly above 30% if only radiative recombination is allowed. This concept was later extended by discussing the effects of non-radiative recombination,[2–6] concentrated incident irradiation,[3,6] and multiple absorbers.[3,7] The principle of detailed balance was further used to derive fundamental correlations of photovoltaic parameters other than PCE; among others, how electroluminescence relates to external quantum efficiency (EQE), and how this aspect can be used to connect the performance of real-world solar cells with theoretical detailed balance calculations.[2,5] Tabulated values for a wide range of single-absorber bandgaps are reported by Rühle.[4] Limitations of the detailed balance limit and a comparison to other theoretical efficiency limits are reported by Markvart.[6]

In this article, we investigate the detailed balance limit of three-terminal tandem solar cells (3T TSCs), which have recently gained scientific interest,[8–26] and for which a record PCE above 29% (certified at 29.56% in two-terminal operation) was presented.[24] For a comprehensive overview of the different types and loading topologies of 3T TSCs, see Warren et al.[17] An overview of the two types of 3 T TSCs that are considered in this article is given in **Figure 1**. Specifically, we want to answer two questions. First, what is the optimum bandgap pairing for 3T TSCs with series (s-type) and antiparallel or reverse (r-type) connected sub-cells in the radiative limit? To our knowledge, this aspect has yet only been investigated for specific combinations of absorber materials (e.g., perovskite on silicon[16] or group III/V semiconductors on silicon[27]) but not in a bandgap-agnostic fashion as it has been shown for two-terminal (2T) and four-terminal (4T) TSCs.[7,28–32] Note that Steiner et al. reported on a theoretical efficiency limit specifically for 3T TSCs based on

P. Wagner, P. Tockhorn, L. Zimmermann, E. Köhnen, F. Scheler, M. Härtel, S. Albrecht, L. Korte
Solar Energy Division
Department Perovskite Tandem Solar Cells
Helmholtz-Zentrum Berlin
12489 Berlin, Germany
E-mail: philipp.wagner@helmholtz-berlin.de; korte@helmholtz-berlin.de

S. Mariotti
Energy Materials and Surface Sciences Unit (EMSSU)
Okinawa Institute of Science and Technology Graduate University (OIST)
Okinawa 904-0495, Japan

S. Albrecht
Fakultät IV – Elektrotechnik und Informatik
Technical University Berlin
Berlin 10587, Germany

The ORCID identification number(s) for the author(s) of this article can be found under https://doi.org/10.1002/solr.202300963.

DOI: 10.1002/solr.202300963

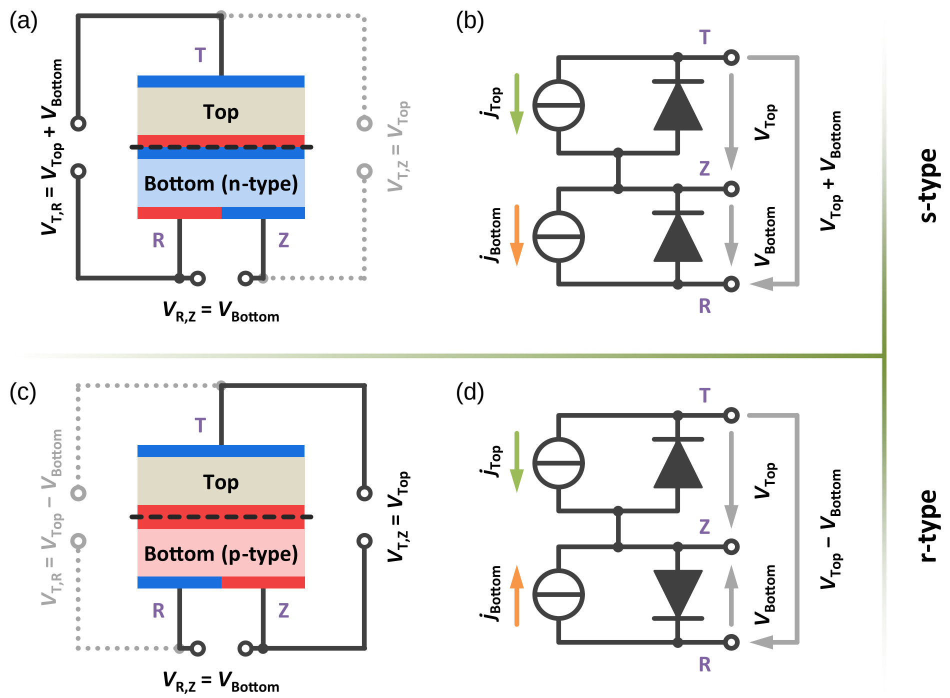

Figure 1. Simplified device schematic and equivalent circuit of a,b) an s-type 3 T TSC and c,d) an r-type 3T TSC as they are considered in this article. T, R, and Z denote the three electrodes of a 3T TSC with interdigitated back-contact (IBC) bottom cell in accordance with ref. [17]. For s-type 3T TSCs, the common R mode is used as loading topology (i.e., electrode R is shared between the two sub-cells), while for r-type 3T TSCs, the common Z mode is used. The respective other mode for each device is shown as dotted grey lines. Dashed black lines separate top and bottom cell. Blue layers represent n-type and red layers p-type materials. Absorber materials, layers configuration, and loading topologies were chosen in accordance with earlier 3T TSCs fabricated within our group.[25] Other materials, layer configurations, and loading topologies are conceivable.[17]

III/V absorber materials for a variety of bandgap combinations of top and bottom cells,[33] but they used an empirical approach under concentrated illumination after ref. [34] instead of a rigorous detailed balance calculation and by using the AM 1.5 g standard spectrum.[35]

The second question is as follows: what is the optimum bandgap pairing for 3T TSCs under the additional constraint of voltage matching? This is a necessary requirement for forming effectively working strings in a 3T solar module.[27,36,37] To this end, we investigate the two most promising voltage-matching ratios (VMRs) of 1:2 and 2:3, meaning the voltage at maximum power point (MPP, V_{MPP}) of one (two) top cell(s) is equal to V_{MPP} of two (three) bottom cells. To obtain realistic values for V_{MPP} as a function of the absorber bandgap, we additionally need to consider non-radiative recombination. This is done by introducing a factor, f_c, as the fraction of radiative-to-total recombination as was already proposed in ref. [1]. We then use data of record and high-efficiency solar cells based on different absorber materials to estimate a meaningful value range for f_c (details are given later) and use these as input for adapted detailed balance calculations that include non-radiative recombination.

2. Methodology

This section gives an overview of the applied procedure to extract limiting efficiencies of 3T TSCs following the principles of detailed balance. If not stated otherwise, we followed the procedures presented in refs. [1,4,5,7]. The full set of used equations can be found in the Supporting Information. Here, we focus only on equations relevant to the subsequent discussion, or those where we want to point out conditions specific to our calculations.

The radiative recombination parameter or saturation current density ($j_{0,rad}$) of the top cell (indexed as "top") is defined by

$$j_{0,\text{rad,top}} = q \cdot \int_{-\infty}^{\infty} H(E) \cdot \varphi_{\text{BB,300K}}(E) dE \tag{1}$$

where q represents the elementary charge, $\varphi_{\text{BB,300 K}}$ represents the photon flux spectrum of an ideal blackbody at 300 K (i.e., the radiation that an ideal solar cell would emit at operation temperature under standard test conditions[5]), and $H(E)$ represents the Heaviside step function (see Supporting Information).

For the bottom cell (indexed as "bottom"), $j_{0,rad}$ is defined in a similar fashion by

$$j_{0,\text{rad,bottom}} = q \cdot \int_{-\infty}^{\infty} \Pi(E) \cdot \varphi_{\text{BB,300K}}(E) dE \tag{2}$$

but by using the rectangular function, $\Pi(E)$ (see Supporting Information). The magnitude of $j_{0,rad}$ is influenced by whether radiation is emitted by both surfaces of a sub-cell (as originally proposed by Shockley and Queisser[1]) or just by the front side (e.g., if the rear side is fully covered by an ideal reflective surface such as a metal contact). This aspect was considered by introducing a geometrical factor, f_g, which can be 1 or 2 accordingly.[4] Equation (1) and (2) inherently assume f_g to be 2 (for an equivalent alternative definition that explicitly includes f_g, see e.g., ref. [4].) In the context of this work, we chose f_g to be 2 and 1 for top and bottom cell, respectively, as the top cell in a 3 T TSC must be semitransparent (and can thus emit radiation from both surfaces) while the bottom cell features a full-area rear-side metallization. This assumption is valid because 1) bifaciality was not considered, and 2) even in interdigitated back-contact (IBC) configuration, the metallized fraction should account for close to 100% of the total rear side area since the metallization gap between minority and majority charge-carrier contacts is usually only a few microns wide. With knowledge of $j_{0,\text{rad}}$, one can calculate full dark current density–voltage (J–V) characteristics of each sub-cell. In combination with the short-circuit current density, j_{sc} (see Supporting Information), all essential solar cell performance parameters can be extracted (see Supporting Information for details).

After having defined the performance of each sub-cell, the MPP of the whole device must be defined. Contrary to 2T or 4T TSCs, voltage and current density at MPP depend on the type of 3T TSC while the overall power output (P) does not: ideally, P is identical for different 3T configurations (r-type or s-type) and loading topologies (i.e., which of the electrodes is shared between both sub-cells).[17,21] In other words, the same power output can be obtained for different devices by adjusting the voltages at which they are biased. So far, however, this aspect was shown only for distinct combinations of absorber materials[21] but was not presented in an absorber-material or bandgap-agnostic fashion. To this end, we investigated the performance of two common types of 3T TSCs that featured either reverse (r-type) or series (s-type) connected sub-cells and shared the IBC bottom cell's electron (hole) contact if its top electrode is a hole (electron) contact (see Figure 1). Although not explicitly investigated, the same results should hold true for 3T TSCs with middle contact as they constitute only a different device architecture and not a fundamentally different operation principle.

For r-type devices in common Z mode, it has been reported that the open-circuit voltage (V_{oc}) of each sub-cell is affected by the operating condition of the other sub-cell. More specifically, the V_{oc} of one sub-cell decreases when more current is extracted through the other sub–cell. This effect was related to a voltage drop across the bottom cell's shared resistance components ($R_{\text{s,bottom,shared}}$) and vanished for $R_{\text{s,bottom,shared}} = 0\,\Omega\,\text{cm}^2$.[16] Since there are no explicit resistive losses in detailed balance limit calculations (as were conducted here), both sub-cells in r-type 3T TSCs can be assumed to operate independently of each other, and their power output at MPP (P_{MPP}) can be described by Equation (3)–(5) with V_{MPP} and j_{MPP} being voltage and current density at MPP.

$$P_{\text{MPP,T,Z}} = P_{\text{MPP,top}} = V_{\text{MPP,top}} \cdot j_{\text{MPP,top}} \tag{3}$$

$$P_{\text{MPP,R,Z}} = P_{\text{MPP,bottom}} = V_{\text{MPP,bottom}} \cdot j_{\text{MPP,bottom}} \tag{4}$$

$$P_{\text{MPP,r-type}} = P_{\text{MPP,top}} + P_{\text{MPP,bottom}} \tag{5}$$

In turn, for s-type devices in common R mode, the electrical circuits of both sub-cells are strongly interdependent, and the device performance cannot be described by single J–V scans of individual sub-cells. Instead, it is best to conceive these types of 3T TSCs as comprising a power-generating sub-circuit (where the voltages across both sub-cells added up, defined by $P_{\text{MPP,T,R}}$) and a current compensating or regulating sub-circuit (where the difference in current densities at MPP is extracted through or injected into the third terminal, defined by $P_{\text{MPP,R,Z}}$). Thus, the power output of s–type 3T TSCs is described by Equation (6)–(8). For a more detailed description of the electrical behavior of s–type 3T TSCs, see ref. [25].

$$P_{\text{MPP,T,R}} = (V_{\text{MPP,top}} + V_{\text{MPP,bottom}}) \cdot j_{\text{MPP,top}} \tag{6}$$

$$P_{\text{MPP,R,Z}} = V_{\text{MPP,bottom}} \cdot (j_{\text{MPP,bottom}} - j_{\text{MPP,top}}) \tag{7}$$

$$P_{\text{MPP,s-type}} = P_{\text{MPP,T,R}} + P_{\text{MPP,R,Z}} \tag{8}$$

Mathematically, Equation (5) and (8) are equivalent (see also Supporting Information), and therefore, the power output of r-type and s-type 3T TSCs is identical. This is also true for loading topologies other than the ones considered here (see Supporting Information). In the following, we will primarily focus on s-type devices as this allows us to use our in-house record s-type 3T TSC as a benchmark.

3. Results and Discussion

3.1. Radiative Efficiency Limit of 3T TSCs

Figure 2a shows the limiting efficiency as a function of sub-cell bandgaps (E_G) for s-type 3T TSCs, calculated as described in the previous section and under the assumption of only radiative recombination. A simplified electrical equivalent circuit of the considered device is depicted as an inset. Results of r-type devices can be found in Figure S2, Supporting Information. For top and bottom cell absorbers, bandgap regions between 1.2–2.3 and 0.9–1.5 eV are considered, and 10 meV is chosen as step size. As a first expected result, the distribution for both r-type and s-type 3T TSCs is identical, which confirms the equivalency of power output reported for specific cases[17,21] as a universal feature of 3T TSCs. This is also true for all other investigated cases presented throughout this article, which is why we will only show the results of s-type devices in the following. Second, the distribution of maximum efficiency (and with it the optimum bandgap pairing) differs quite substantially for 3T and 2T TSCs (compare to ref. [31]). In 3T TSCs, not choosing the optimum bandgap combination is more forgiving compared to 2T TSCs as the window for achieving very high efficiencies is generally wider around the optimum. In fact, the distribution shown in Figure 2a is identical to that reported for 4T TSCs (compare to ref. [31]) because current matching is not necessary in both 3T and 4T TSCs. This makes 3T TSCs as flexible as 4T TSCs in terms of absorber material choice. A maximum PCE of 45.6% is achieved for a bandgap pairing of 1.73 eV for the top cell and 0.94 eV for the bottom cell. For some popular absorber material combinations for TSCs, $E_{\text{G,top}}$, $E_{\text{G,bottom}}$, and combined PCE are listed in **Table 1** together with suggested further literature in which they have been used.

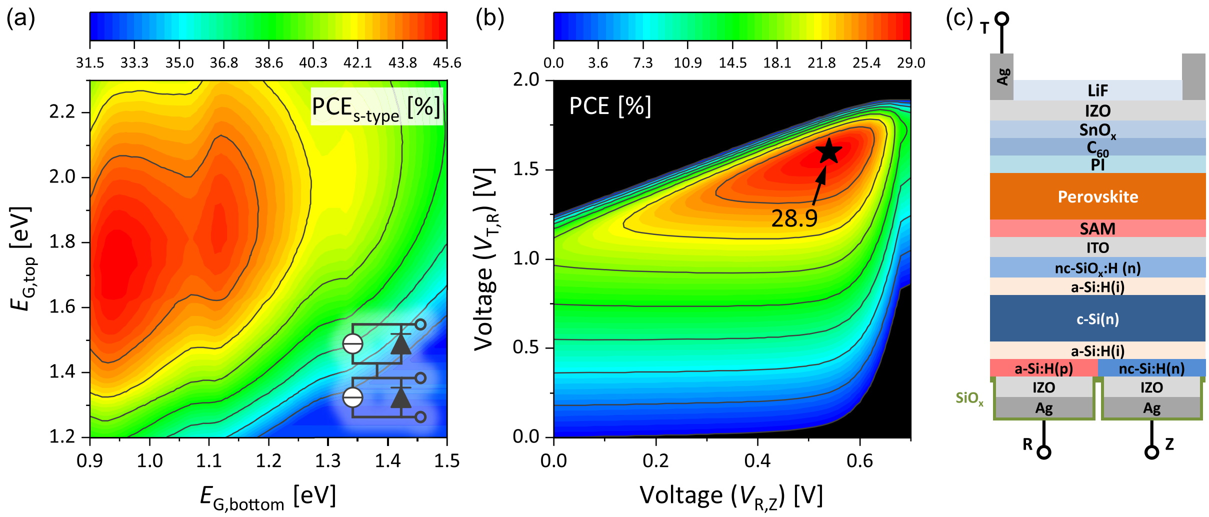

Figure 2. a) Limiting efficiency as a function of top and bottom cell bandgap of an ideal s-type 3T TSC. A simplified electrical equivalent circuit model is depicted as an inset (see also Figure 1b). b) Measured efficiency map of our current in-house record s-type 3T TSC with perovskite top and IBC silicon heterojunction (SHJ) bottom cell. The MPP is marked with a black star and a maximum PCE of 28.9% is obtained. c) Schematic (not to scale) of the used layer stack (further details are given in Supporting Information).

Table 1. Optimal bandgaps and detailed balance efficiencies of 3 T TSCs calculated by the method presented earlier for a selection of popular absorber material choices in tandem solar cells. The following abbreviations are used: CIGS (copper indium gallium (di)selenide) and GaInP (gallium indium phosphide).

Absorber combination	$E_{G,top}$ [eV]	$E_{G,bottom}$ [eV]	PCE [%]	Further literature on absorber combination
Perovskite–silicon	1.82	1.12	44.8	[38,79]
Perovskite–CIGS	1.81	1.05[a)]	44.5	[80,81]
All-perovskite	1.92	1.22[b)]	43.1	[68,69]
GaInP–silicon	1.80	1.12	44.8	[11,12]

[a)]Bandgap assumed in accordance with ref. [49]. [b)]Bandgap assumed in accordance with ref. [69].

For the case of perovskite-on-silicon 3T TSCs, we present our best s-type device with a combined PCE of 28.9%. This experimental realization is used (among other record efficiency devices) to derive a realistic parameterization for the inclusion of non-radiative recombination into our model (see next section). Figure 2b shows the efficiency map and Figure 2c a schematic of the employed layer stack of this device. Details on its fabrication can be found in the Supporting Information. The characterization procedure to extract the efficiency map is described in detail in ref. [25]. The same perovskite top cell stack has also recently been used in a high-efficiency 2T TSC[38] with hole-collecting contact as described in ref. [39]. More details on the fabrication of the IBC bottom cell can be found in ref. [40] as well as in Supporting Information.

3.2. Efficiency Limit of 3T TSCs for Voltage-Matched Strings

Another important aspect that was highlighted in recent literature is the necessity of voltage-matching sub-cells to form strings in a 3T solar module.[27,36,37] Here, the condition $m \times V_{\mathrm{MPP,top}} = n \times V_{\mathrm{MPP,bottom}}$ must be met, with m and n being the amount of top and bottom cells, respectively, connected in series. The two most promising VMRs, m:n, for potential industrial applications that are discussed in literature are 1:2 and 2:3.[36,37] Other VMRs are conceivable but will result in higher end-of-string losses.[37] It has further been argued that r-type 3T TSCs might be more attractive for industrial applications because of potentially lower interconnection complexity.[37]

This implies that the absorber materials in 3T TSCs might have to be chosen more carefully than the initial detailed balance calculations suggest. To find the optimum bandgap pairing for 3T TSCs under voltage-matching constraints while simultaneously achieving a high PCE, assumptions about non-radiative recombination must be made to obtain realistic device voltages. V_{oc}s and V_{MMP}s under radiative limit conditions are too high for this purpose and might give misleading results.

As j_0 varies with bandgap and the magnitude of non-radiative recombination, Shockley and Queisser introduced a factor, f_c, that represents the ratio of radiative recombination to total recombination; see Equation (9).[1,4] This factor is also referred to as light-emitting diode (LED) quantum efficiency of a solar cell in ref. [2], where it is shown that it can be linked directly to the V_{oc} of real-world devices.

$$f_c = \frac{F_{c0}}{F_{c0} + R(0)} \tag{9}$$

F_{c0} and $R(0)$ represent the radiative and non-radiative recombination rate, respectively. In the radiative limit (see previous section), f_c is 1 per definition since there is no non-radiative recombination under detailed balance conditions. With values lower than 1, f_c acts as a linear scaling factor for j_0 (see Supporting Information). In a next step, we need to find a meaningful value (or value range) for f_c. In our case, we are mostly interested in obtaining realistic voltage values, thus it would be most beneficial to match V_{MPP}s of real and calculated devices. However, most publications on record and high-efficiency devices do not include this parameter. We therefore choose V_{oc} as a proxy and assume a similar absolute reduction of both quantities for decreasing f_{c}. Next, we calculate limiting efficiencies of single-junction solar cells for f_{c}s of 0.1, 0.01, and 0.001 (solid lines in **Figure 3**) and compare the resulting ratios of $V_{\mathrm{oc}}/V_{\mathrm{oc,rad}}$ to those of real record and high-efficiency devices for different categories of typical absorber materials (symbols in Figure 3, details on specific devices are given in the figure caption and Supporting Information). Absorber materials that would normally be used as a top cell in tandem devices are marked with open symbols and those used as bottom cell materials with closed symbols. Half-open symbols (cadmium telluride, CdTe, and gallium arsenide, GaAs) represent materials that can likely be used as either sub-cell. The sub-cells of our in-house record s-type 3T TSC are represented with a blue and a grey star for perovskite top cell and IBC SHJ bottom cell, respectively.

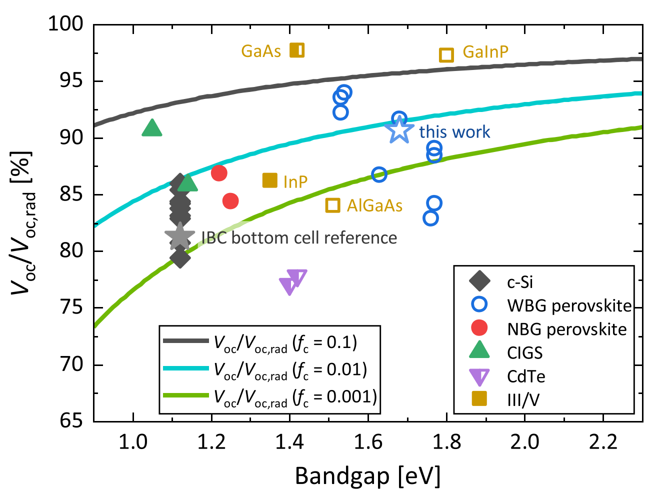

Figure 3. Calculated $V_{\mathrm{oc}}/V_{\mathrm{oc,rad}}$ ratios of single-junction solar cells as a function of bandgap and f_{c} (solid lines), and $V_{\mathrm{oc}}/V_{\mathrm{oc,rad}}$ ratios of real-world record and high-efficiency solar cells reported in literature (symbols). For better comparability, f_{g} is set to 1 for all devices in this graph. Device parameters are taken from the National Renewable Energy Laboratory (NREL) chart[60] or efficiency tables[50] (including its earlier iterations) as well as the following publications (in addition to the former): crystalline silicon (c–Si),[40,61–67] CIGS,[49] narrow-bandgap (NBG), and wide-bandgap (WBG) perovskite,[25,38,68–74] indium phosphide (InP),[75] GaAs,[76] and aluminum gallium arsenide (AlGaAs).[77] NBG and WBG perovskites are defined in accordance with refs. [42,52], respectively. Where not explicitly mentioned in the original publication, the bandgap is estimated from the inflection point at the absorption edge of the EQE as described in ref. [78]. If the EQE is not included in the original publication, the one reported in ref. [50] or one of its earlier iterations is used. For details as well as tabulated data of the included devices we refer to Table S1, Supporting Information. Open symbols represent typical top cell absorbers, closed symbols bottom cell absorbers, and half-open symbols absorbers that can be used as either top or bottom cell. The data point highlighted with a blue star marks the perovskite top cell of our current in-house record 3T TSC (see Figure 2b). A single-junction equivalent of the corresponding IBC SHJ bottom cell (marked with a grey star) has been presented in ref. [40].

For most investigated technologies, choosing f_{c} between 0.1 and 0.001 gives a good agreement between V_{oc}s of real and calculated devices. However, there are some notable exceptions: record devices with the III/V absorber materials GaAs and gallium indium phosphide (GaInP) almost reach their respective radiative V_{oc} limit whereas CdTe and some wide-bandgap (WBG) perovskites feature exceptionally low $V_{\mathrm{oc}}/V_{\mathrm{oc,rad}}$ ratios. For CdTe, relatively low V_{oc}s are a known issue that stem from a high density of intrinsic defects in the absorber material, which in turn result in low hole densities and minority charge-carrier lifetimes.[41] For WBG perovskites, this is case-specific since very high $V_{\mathrm{oc}}/V_{\mathrm{oc,rad}}$ ratios have also be achieved for absorbers with bandgaps above 1.70 eV.[42,43] With the exception of some WBG absorbers, such as perovskites, where a larger V_{oc} deficit is sometimes found in real devices, absorber materials with wider bandgaps are generally less affected by voltage losses due to a lower f_{c} (solid lines in Figure 3). In the dark, this is due to the exponentially decreasing minority charge-carrier concentration in absorbers with wider bandgaps. Additionally, non-radiative recombination is reported to become less prominent in wider bandgap absorbers.[44] Thus, in high-performance devices, absorber materials that are typically considered for top cells seem to agree more with an f_{c} range of 0.1–0.01, and bottom cell materials with an f_{c} range of 0.01–0.001. We therefore set $f_{\mathrm{c,top}}$ to 0.1 and $f_{\mathrm{c,bottom}}$ to 0.01 to get a realistic upper efficiency limit of 3T TSCs (in terms of V_{oc}) for voltage-matched strings. Other f_{c} combinations have been simulated as well (see Figure S3, Supporting Information), and general trends will be discussed in the next section. **Figure 4**a shows the maximum efficiency versus top and bottom cell absorber bandgap when the effects of non-radiative recombination are taken into account. Possible bandgap pairings for VMRs of 1:2 and 2:3 are marked with black and red lines, respectively, and their shaded areas indicate 99% prediction bands (for more details, see Figure S4, Supporting Information). The bandgap pairing that yields the highest efficiency in each case is marked with a star. A blue diamond highlights the bandgap combination of our present in-house record 3T TSC (Figure 2b). To achieve voltage matching with a VMR of 1:2 for this specific device, a wider top cell bandgap would be required, which additionally increases the theoretical PCE potential by approximately 0.4%$_{\mathrm{abs}}$.

Under the given assumptions, the optimum bandgap pairing for a VMR of 1:2 is 1.79 eV for the top cell and 1.12 eV for the bottom cell with a maximum combined PCE of 40.9%, which could be satisfied by a WBG perovskite or (slightly bandgap-tuned[45]) GaInP on crystalline silicon or copper indium gallium (di)selenide (CIGS). For a VMR of 2:3, the results are 1.74 eV (WBG perovskite or bandgap-tuned GaInP) for the top cell, 1.34 eV (narrow-bandgap [NBG] perovskite, CIGS, or InP) for the bottom cell, and a maximum overall PCE of 37.9%. This is different from the optimum in the radiative limit for both the global optimum case and under voltage-matching constraints (see previous section and Figure 4b). It should be noted that here, no resistance-related losses are considered. In real devices, these losses need to be accounted for, which could result in optimum bandgap pairings (and efficiencies) different from the ones reported here. The inclusion of these losses (especially of series resistance, R_{s}) would also demand different definitions for J–V characteristics and

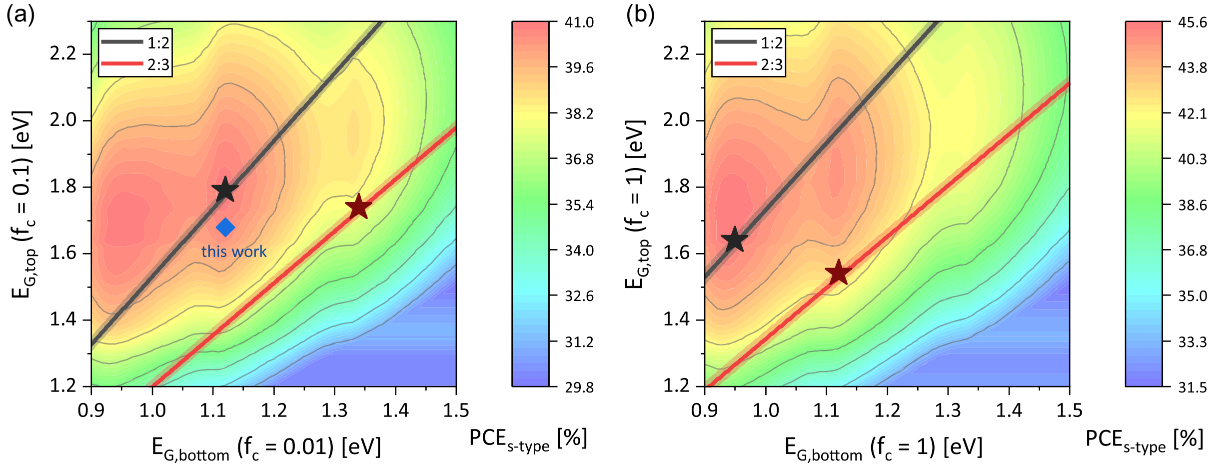

Figure 4. Limiting efficiency as a function of top and bottom cell bandgap: a) considering non-radiative recombination ($f_{c,top} = 0.1$, $f_{c,bottom} = 0.01$) of an otherwise ideal s-type 3T TSC, b) in the radiative efficiency limit ($f_{c,top} = f_{c,bottom} = 1$). Black (red) lines show potential bandgap pairings for a VMR of 1:2 (2:3) with 99% prediction bands as shaded areas. Stars mark the optimum combination with the highest attainable PCE under voltage-matching constraints in each case. The bandgap combination of our current in-house record 3T TSC (see Figure 2b) is marked with a blue diamond.

MPPs of r-type and s-type 3T TSCs since with a finite R_s, sub-cells/sub-circuits show a stronger interdependence than without.[16] However, considering resistance-related losses is beyond the scope of this article.

Other possible combinations for both VMRs that do not yield the optimum bandgap pairing are tabulated in Tables S2 and S3, Supporting Information, together with suggestions for possible absorber materials. In general, the following absorber materials could be used for distinct simulated bandgap regions. As for most ternary III/V semiconductors, the bandgap of InGaAs can continuously be tuned between that of InAs (0.36 eV) and GaAs (1.42 eV) by changing the stoichiometry toward either of its two components as shown in ref. [46, ch. 3], which makes it a good choice for bottom cells with bandgaps below 1.00 eV. Typically, a composition with a bandgap of 0.75 eV is chosen to avoid mechanical strain during epitaxial growth due to lattice mismatch with InP substrates.[47] When using different compositions to tune the bandgap, additional lattice-grading layers must be employed. The bandgap region between 1.00 and 1.70 eV can be covered by CIGS in different compositions,[48] with the highest single-junction PCEs having been achieved with absorbers bandgaps below 1.10 eV[49,50] and the global maximum PCE being predicted for about 1.50 eV.[51] Tin or mixed tin–lead-based NBG perovskites occupy the same bandgap region: their bandgap can be tuned between 1.20 and 1.60 eV but is usually in the range of 1.20–1.40 eV.[52–54] Crystalline silicon (1.12 eV), InP (1.35 eV), GaAs (1.42 eV), and CdTe (1.50 eV) also fall into this region. Alloying CdTe with selenium can narrow the absorber bandgap to 1.39 eV[55] while using zinc as an alloying element can widen the bandgap up to 2.44 eV (a device with up to 1.82 eV has been experimentally demonstrated).[29,56] For bandgaps above 1.50 eV, different compositions of lead-based WBG perovskites are a good choice as they cover a wide range.[42] AlGaAs (with a tunable bandgap from 1.42 to 2.17 eV as reported in ref. [46, ch. 1]) is another attractive top cell material.[57] With 1.80 eV (tunable between 1.65 and 1.82 eV[45]), GaInP features an almost optimum bandgap for various potential bandgap pairings and is therefore used as top cell absorber in many III/V-on-silicon-based 2T and 3T TSCs.[11–13,18,23,36,58,59]

3.3. Impact of Non-Radiative Recombination on Maximum Efficiency and Optimum Bandgap Pairing

Lastly, we investigate general trends for the impact of different combinations of $f_{c,top}$ and $f_{c,bottom}$ (as described in the previous section) on maximum attainable PCE (**Figure 5**a,b), either globally (designated as PCE_{max}) or under voltage-matching constraints ($PCE_{VM(1:2)}$ and $PCE_{VM(2:3)}$), and on optimum bandgap pairing for VMRs of 1:2 and 2:3 (Figure 5c,d). Results are shown for fixed $f_{c,top}$ and varied $f_{c,bottom}$ (Figure 5a,c) and for fixed $f_{c,bottom}$ and varied $f_{c,top}$ (Figure 5b,d). A 3×3 matrix showing efficiency maps as a function of sub-cell bandgaps, similar to those presented in Figure 4, can be found in Figure S3, Supporting Information, for all calculated f_c combinations and investigated voltage-matching cases. For an overview of realistic values of f_c attainable with specific absorber materials, see Figure 3. For every given simulated top cell with a fixed $f_{c,top}$, PCE_{max}, and PCE_{VM} for both VMRs decrease exponentially for lower $f_{c,bottom}$ (i.e., for increasing non-radiative recombination) (Figure 5a). The same holds true for fixed $f_{c,bottom}$ and decreasing $f_{c,top}$ but to a lesser extent (Figure 5b). The PCE of the 1:2 voltage-matched case follows the development of the global optimum PCE well for all investigated variations of both f_cs. This means that, for the 1:2 case, there is almost no power loss (at most $0.4\%_{abs}$ in PCE) in spite of additional voltage-matching constraints (see also Figure S5, Supporting Information, where the PCE loss, defined as $PCE_{VM} - PCE_{max}$, is depicted for both VMRs as a function of $f_{c,top}$ and $f_{c,bottom}$). This strongly implies that the findings of energy yield calculations based on unconstrained tandem solar cells that predict an advantage in annual energy yield for 3T TSCs over 2T TSCs[19,20] are still valid under voltage-matching conditions, at least when using a VMR of 1:2. Furthermore, optimum bandgaps ($E_{G,opt}$) for PCE_{max} of both top

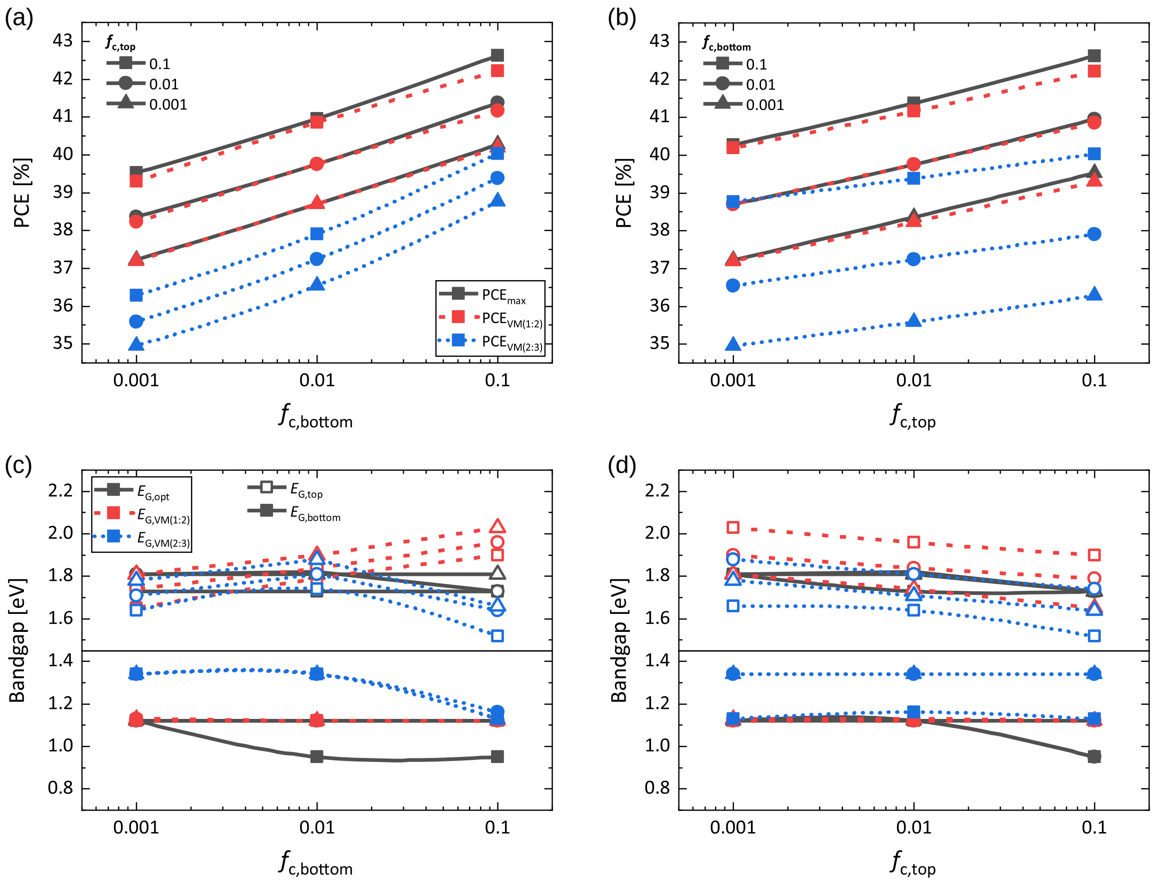

Figure 5. Impact of f_c on a,b) maximum attainable PCE, and c,d) optimum bandgap pairing. Three cases are investigated: a global optimum without voltage-matching constraints (solid black lines), a voltage-matching ratio of 1:2 (dashed red lines), and a voltage-matching ratio of 2:3 (dotted blue lines). (a) and (c) show results for fixed $f_{c,top}$ and varying $f_{c,bottom}$ while (b) and (d) show results for fixed $f_{c,bottom}$ and varying $f_{c,top}$. In each case, f_c is fixed to 0.1 (squares), 0.01 (circles), and 0.001 (triangles). In (c) and (d), a horizontal line separates top (open symbols) and bottom cell (closed symbols) bandgaps. Tabulated data are included in Table S4, Supporting Information. Note the logarithmic scale of all abscissae. Graphs (a) and (b) as well as (c) and (d) share legends regarding PCE and bandgap.

and bottom cell shift slightly toward higher values (compared with the radiative limit) and plateau at about 1.81 and 1.12 eV, respectively, when the rate of non-radiative recombination increases (i.e., when both f_cs decrease) (Figure 5c,d). This is to compensate for higher voltage losses associated with narrower bandgaps at a lower f_c as discussed in the previous section (see Figure 3). In contrast to that, the optimum top cell bandgap for a VMR of 1:2 shifts to lower values if the quality of the bottom cell deteriorates (for a decreasing $f_{c,bottom}$) and to higher values for increased non-radiative recombination in the top cell (decreasing $f_{c,top}$) while the optimum bottom cell bandgap stays unchanged at 1.12 eV in either case (Figure 5c,d). For a VMR of 2:3, $E_{G,top}$ features a local maximum for $f_{c,bottom} = 0.01$ when $f_{c,top}$ is fixed (Figure 5c), or it increases for decreasing $f_{c,top}$ when $f_{c,bottom}$ is fixed (Figure 5d). In contrast, $E_{G,bottom}$ increases from 1.13 to 1.34 eV when $f_{c,bottom}$ decreases. More generally, there is a linear dependence of the two bandgaps in 3T TSCs that allows for voltage matching (straight lines in Figure 4 and S3, Supporting Information). These lines shift to wider bandgaps (for both top and bottom cell absorber) for decreasing $f_{c,top}$ and $f_{c,bottom}$ (i.e., when the rate of non-radiative recombination increases), and the maximum attainable PCE in each case can be determined from the corresponding PCE map. As can be seen in the graphs, voltage losses due to higher recombination rates are compensated by a higher voltage potential of a wider bandgap absorber.

4. Conclusions

3T TSCs show a remarkable PCE potential with a sub-cell bandgap versus efficiency distribution identical to that of 4T TSCs. In the radiative limit, a maximum PCE of 45.6% can be achieved for a top cell with 1.73 eV and a bottom cell with 0.94 eV. Also, there is no difference in the efficiency distribution of r-type and s-type 3T TSCs, which exemplifies the equivalency in power output of different device types and loading topologies reported for specific cases. So far, a maximum PCE of 29% (certified at 29.56% in 2T configuration) has been reported in literature.[24] Here, we present a perovskite–silicon 3T TSC on a comparably high efficiency level of 28.9%. To assess the optimum bandgap pairing for 3T TSCs in voltage-matched strings, which are necessary for module integration of 3T TSCs, non-radiative recombination is considered by employing a radiative-to-total recombination factor, f_c, and quantifying it with the V_{oc}s of real-world record and high-efficiency single-junction solar cells based on different absorber materials. When choosing realistic values for f_c, we find the optimum bandgap pairing for top and bottom cell and a VMR of 1:2 to be 1.79 and 1.12 eV, respectively, with a maximum attainable PCE of 40.9%. For a VMR of 2:3, these values are 1.74, 1.34 eV, and 37.9%, respectively. The determined optimum bandgap pairings for such sub-cells are well within the range of typical absorber materials. In general, WBG perovskites and GaInP are ideal top cell candidates while crystalline silicon, CIGS, NBG perovskites, and InP are ideal bottom cell candidates for 3T TSCs in voltage-matched strings with VMRs of 1:2 or 2:3. Under voltage-matched conditions, optimum top and bottom cell bandgaps are always larger than in the radiative limit. Compared to the global optimum without voltage-matching constraints, we further find that for a VMR of 1:2 only a small drop of at most $0.4\%_{abs}$ in attainable PCE occurs, which especially holds true for top and bottom cells with non-ideal properties. If a VMR of 2:3 is used, PCE losses can be as high as $1.5\%_{abs}$–$3.3\%_{abs}$ compared to the unconstrained optimum case. From a bandgap engineering perspective, a 1:2 pairing should thus be favored over other possible VMRs for 3 T stringing. In this case, the negligible PCE loss due to the requirement of voltage matching entails that existing energy yield calculations based on single three-terminal tandem solar cells also hold true for voltage-matched strings with a VMR of 1:2. When choosing adequate bandgaps for both top and bottom cell, voltage–matching constraints do not impose a major detriment on 3T TSCs compared to other tandem technologies as power loss can be kept at a very low level. The procedure presented here is easily adaptable to other specific cases by adjusting the ratio of radiative-to-total recombination to match the absorber materials under investigation. Lastly, the findings reported here have further implications for energy yield models and generally the comparison between 2T and 3T TCSs. For a fair comparison of the two tandem architectures, the optimum bandgap pairing for each technology should be used, instead of using a combination that is optimal only for 2T TSCs, in contrast to the approach found so far in literature.

Supporting Information

Supporting Information is available from the Wiley Online Library or from the author.

Acknowledgements

The authors thank their colleagues Anna Belen Morales Vilches, Tobias Henschel, and Kerstin Jacob for silicon wafer texturing and cleaning as well as Carola Ferber, Johannes Beckedahl, and Hagen Heinz for their support in the HySPRINT lab where the perovskite top cell of this study was fabricated. Matthias Zelt is acknowledged for his support with the used PECVD cluster tool. Silicon bottom cell deposition and measurement equipment were provided by the HZB institute PVcomB. The authors further thank their former colleague Sebastian Hall for his assistance with current–voltage measurements of the here investigated device. The authors acknowledge funding provided by the German Federal Ministry of Education and Research (BMBF) through the program "Materialforschung für die Energiewende" (grant no. 03SF0540) and the projects PrEsto (grant no. 03EE1086C), SHAPE (grant no. 03EE1123C), and PEROWIN (grant no. 03SF0631) as well as the Helmholtz Association within the project HySPRINT Innovation Lab. S.M. acknowledges funding provided by JSPS KAKENHI (grant no. JP21F21754) and the Alexander von Humboldt Foundation.

Conflict of Interest

The authors declare no conflict of interest.

Data Availability Statement

The data that support the findings of this study are available from the corresponding author upon reasonable request.

Keywords

detailed balance limit, limiting efficiency, tandem solar cells, three-terminal, voltage matching

Received: November 24, 2023
Revised: December 13, 2023
Published online: January 29, 2024

[1] W. Shockley, H. J. Queisser, *J. Appl. Phys.* **1961**, *32*, 510.
[2] T. Kirchartz, U. Rau, *Phys. Status Solidi A* **2008**, *205*, 2737.
[3] H. J. Queisser, *Mater. Sci. Eng., B* **2009**, *159*, 322.
[4] S. Rühle, *Sol. Energy* **2016**, *130*, 139.
[5] U. Rau, B. Blank, T. C. M. Müller, T. Kirchartz, *Phys. Rev. Appl.* **2017**, *7*, 044016.
[6] T. Markvart, *Wiley Interdiscip. Rev.: Energy Environ.* **2022**, *11*, e430.
[7] A. De Vos, *J. Phys. D: Appl. Phys.* **1980**, *13*, 839.
[8] S. Sakai, M. Umeno, *J. Appl. Phys.* **1980**, *51*, 5018.
[9] T. Nagashima, K. Okumura, K. Murata, Y. Kimura, in *Conf. Record of the Twenty-Eighth IEEE Photovoltaic Specialists Conf.-2000 (Cat. No. 00CH37036)*, IEEE, Piscataway, NJ **2000**, pp. 1193–1196.
[10] G. W. P. Adhyaksa, E. Johlin, E. C. Garnett, *Nano Lett.* **2017**, *17*, 5206.
[11] E. L. Warren, M. G. Deceglie, M. Rienäcker, R. Peibst, A. C. Tamboli, P. Stradins, *Sustainable Energy Fuels* **2018**, *2*, 1141.
[12] M. Schnabel, M. Rienäcker, E. L. Warren, J. F. Geisz, R. Peibst, P. Stradins, A. C. Tamboli, *IEEE J. Photovoltaics* **2018**, *8*, 1584.
[13] Z. Djebbour, W. El-Huni, A. Migan Dubois, J.-P. Kleider, *Prog. Photovoltaics* **2019**, *27*, 306.
[14] I. J. Park, J. H. Park, S. G. Ji, M.-A. Park, J. H. Jang, J. Y. Kim, *Joule* **2019**, *3*, 807.
[15] M. Rienäcker, E. L. Warren, M. Schnabel, H. Schulte-Huxel, R. Niepelt, R. Brendel, P. Stradins, A. C. Tamboli, R. Peibst, *Prog. Photovoltaics* **2019**, *27*, 410.
[16] P. Tockhorn, P. Wagner, L. Kegelmann, S. M. Mews, S. Albrecht, L. Korte, *ACS Appl. Energy Mater.* **2020**, *3*, 1381.
[17] E. L. Warren, W. E. McMahon, M. Rienacker, K. T. VanSant, R. C. Whitehead, R. Peibst, A. C. Tamboli, *ACS Energy Lett.* **2020**, *5*, 1233.
[18] M. Schnabel, H. Schulte-Huxel, M. Rienäcker, E. L. Warren, P. F. Ndione, B. Nemeth, T. R. Klein, M. F. A. M. Van Hest, J. F. Geisz, R. Peibst, P. Stradins, A. C. Tamboli, *Sustainable Energy Fuels* **2020**, *4*, 549.
[19] H. Liu, C. D. Rodríguez-Gallegos, Z. Liu, T. Buonassisi, T. Reindl, I. M. Peters, *Cell Rep. Phys. Sci.* **2020**, *1*, 100037.

[20] F. Gota, M. Langenhorst, R. Schmager, J. Lehr, U. W. Paetzold, *Joule* **2020**, *4*, 2387.
[21] T. Tayagaki, K. Makita, T. Tachibana, H. Mizuno, R. Oshima, H. Takato, T. Sugaya, *Sol. Energy Mater. Sol. Cells* **2021**, *221*, 110901.
[22] J. H. Park, S. G. Ji, I. J. Park, S. K. Hwang, H. W. Lim, J. Y. Kim, *Cell Rep. Phys. Sci.* **2022**, *3*, 101076.
[23] K. T. VanSant, E. L. Warren, J. F. Geisz, T. R. Klein, S. Johnston, W. E. McMahon, H. Schulte-Huxel, M. Rienäcker, R. Peibst, A. C. Tamboli, *Iscience* **2022**, *25*, 104950.
[24] L. Senaud, B. Kamino, J. Geissbühler, G. Christmann, F. Sahli, P. Wyss, D. L. Bätzner, D. Lachenal, Q. Jeangros, C. Ballif, B. Paviet-Salomon, C. Allebé, M. Kikelj, presented at *8th World Conf. Photovoltaic Energy Conversion (WCPEC-8)*, Milan, Italy, **2022**.
[25] P. Wagner, P. Tockhorn, S. Hall, S. Albrecht, L. Korte, *Sol. RRL* **2023**, *7*, 2200954.
[26] L. Dai, S. Li, Y. Hu, J. Huang, Z. Liu, H. Shi, G. Guan, Y. Shen, B. Hu, P. R.I. Cabarrocas, M. Wang, *ACS Energy Lett.* **2023**, *8*, 3839.
[27] H. Schulte-Huxel, D. J. Friedman, A. C. Tamboli, *IEEE J. Photovoltaics* **2018**, *8*, 1370.
[28] M. E. Nell, A. M. Barnett, *IEEE Trans. Electron Devices* **1987**, *34*, 257.
[29] Z. J. Yu, M. Leilaeioun, Z. Holman, *Nat. Energy* **2016**, *1*, 16137.
[30] M. H. Futscher, B. Ehrler, *ACS Energy Lett.* **2016**, *1*, 863.
[31] T. Leijtens, K. A. Bush, R. Prasanna, M. D. McGehee, *Nat. Energy* **2018**, *3*, 828.
[32] M. I. Hossain, W. Qarony, S. Ma, L. Zeng, D. Knipp, Y. H. Tsang, *Nano-Micro Lett.* **2019**, *11*, 58.
[33] M. A. Steiner, M. W. Wanlass, J. J. Carapella, A. Duda, J. S. Ward, T. E. Moriarty, K. A. Emery, *Prog. Photovoltaics* **2009**, *17*, 587.
[34] M. W. Wanlass, T. J. Coutts, J. S. Ward, K. A. Emery, T. A. Gessert, C. R. Osterwald, in *The Conf. Record of the Twenty-Second IEEE Photovoltaic Specialists Conf. -1991*, IEEE, Piscataway, NJ **1991**.
[35] National Renewable Energy Laboratory, https://www.nrel.gov/grid/solar-resource/spectra-am1.5.html (accessed: August 2023).
[36] W. E. McMahon, H. Schulte-Huxel, J. Buencuerpo, J. F. Geisz, M. S. Young, T. R. Klein, A. C. Tamboli, E. L. Warren, *IEEE J. Photovoltaics* **2021**, *11*, 1078.
[37] H. Schulte-Huxel, R. Wittek, S. Blankemeyer, M. Köntges, *Prog. Photovoltaics* **2022**, *31*, 1350.
[38] S. Mariotti, E. Köhnen, F. Scheler, K. Sveinbjörnsson, L. Zimmermann, M. Piot, F. Yang, B. Li, J. Warby, A. Musiienko, D. Menzel, F. Lang, S. Keßler, I. Levine, D. Mantione, A. Al-Ashouri, M. S. Härtel, K. Xu, A. Cruz, J. Kurpiers, P. Wagner, H. Köbler, J. Li, A. Magomedov, D. Mecerreyes, E. Unger, A. Abate, M. Stolterfoht, B. Stannowski, R. Schlatmann, et al., *Science* **2023**, *381*, 63.
[39] A. Al-Ashouri, M. Marcinskas, E. Kasparavicius, T. Malinauskas, A. Palmstrom, V. Getautis, S. Albrecht, M. D. McGehee, A. Magomedov, *ACS Energy Lett.* **2023**, *8*, 898.
[40] P. Wagner, A. Cruz, J.-C. Stang, L. Korte, *IEEE J. Photovoltaics* **2021**, *11*, 914.
[41] J. M. Burst, J. N. Duenow, D. S. Albin, E. Colegrove, M. O. Reese, J. A. Aguiar, C.-S. Jiang, M. K. Patel, M. M. Al-Jassim, D. Kuciauskas, S. Swain, T. Ablekim, K. G. Lynn, W. K. Metzger, *Nat. Energy* **2016**, *1*, 16015.
[42] R. He, S. Ren, C. Chen, Z. Yi, Y. Luo, H. Lai, W. Wang, G. Zeng, X. Hao, Y. Wang, J. Zhang, C. Wang, L. Wu, F. Fu, D. Zhao, *Energy Environ. Sci.* **2021**, *14*, 5723.
[43] J. Thiesbrummel, F. Peña-Camargo, K. O. Brinkmann, E. Gutierrez-Partida, F. Yang, J. Warby, S. Albrecht, D. Neher, T. Riedl, H. J. Snaith, M. Stolterfoht, F. Lang, *Adv. Energy Mater.* **2023**, *13*, 2202674.
[44] A. Alkauskas, C. E. Dreyer, J. L. Lyons, C. G. Van de Walle, *Phys. Rev. B* **2016**, *93*, 201304.
[45] I. E. Hashem, C. Zachary Carlin, B. G. Hagar, P. C. Colter, S. M. Bedair, *J. Appl. Phys.* **2016**, *119*, 095706-1.
[46] M. E. Levinshtein, S. L. Rumyantsev, M. S. Shur, *Handbook Series on Semiconductor Parameters, Vol. 2: Ternary and Quaternary III–V Compon Ands*, World Scientific Publishing Co. Pte. Ltd., Singapore **1999**.
[47] Y. Takeda, A. Sasaki, Y. Imamura, T. Takagi, *J. Appl. Phys.* **1976**, *47*, 5405.
[48] N. Rezaei, P. Procel, M. Simor, Z. Vroon, M. Zeman, O. Isabella, *Prog. Photovoltaics* **2020**, *28*, 899.
[49] M. Nakamura, K. Yamaguchi, Y. Kimoto, Y. Yasaki, T. Kato, H. Sugimoto, *IEEE J. Photovoltaics* **2019**, *9*, 1863.
[50] M. A. Green, E. D. Dunlop, M. Yoshita, N. Kopidakis, K. Bothe, G. Siefer, X. Hao, *Prog. Photovoltaics* **2023**, *31*, 651.
[51] C.-H. Huang, *J. Phys. Chem. Solids* **2008**, *69*, 330.
[52] C. Wang, Z. Song, C. Li, D. Zhao, Y. Yan, *Adv. Funct. Mater.* **2019**, *29*, 1808801.
[53] Z. Yang, Z. Yu, H. Wei, X. Xiao, Z. Ni, B. Chen, Y. Deng, S. N. Habisreutinger, X. Chen, K. Wang, J. Zhao, P. N. Rudd, J. J. Berry, M. C. Beard, J. Huang, *Nat. Commun.* **2019**, *10*, 4498.
[54] X. Luo, T. Wu, Y. Wang, X. Lin, H. Su, Q. Han, L. Han, *Sci. China Chem.* **2021**, *64*, 218.
[55] J. Yang, S.-H. Wei, *Chin. Phys. B* **2019**, *28*, 086106.
[56] J. W. Garland, T. Biegala, M. Carmody, C. Gilmore, S. Sivananthan, *J. Appl. Phys.* **2011**, *109*, 102423-1.
[57] K. Tanabe, K. Watanabe, Y. Arakawa, *Sci. Rep.* **2012**, *2*, 349.
[58] S. Essig, C. Allebé, T. Remo, J. F. Geisz, M. A. Steiner, K. Horowitz, L. Barraud, J. S. Ward, M. Schnabel, A. Descoeudres, D. L. Young, M. Woodhouse, M. Despeisse, C. Ballif, A. Tamboli, *Nat. Energy* **2017**, *2*, 17144.
[59] W. E. McMahon, J. F. Geisz, J. Buencuerpo, E. L. Warren, *Sustainable Energy Fuels* **2023**, *7*, 461.
[60] National Renewable Energy Laboratory, https://www.nrel.gov/pv/cell-efficiency.html, (accessed: August 2023).
[61] M. A. Green, *Prog. Photovoltaics* **2009**, *17*, 183.
[62] J. Nakamura, N. Asano, T. Hieda, C. Okamoto, H. Katayama, K. Nakamura, *IEEE J. Photovoltaics* **2014**, *4*, 1491.
[63] K. Yoshikawa, H. Kawasaki, W. Yoshida, T. Irie, K. Konishi, K. Nakano, T. Uto, D. Adachi, M. Kanematsu, H. Uzu, K. Yamamoto, *Nat. Energy* **2017**, *2*, 17032.
[64] A. Richter, J. Benick, F. Feldmann, A. Fell, M. Hermle, S. W. Glunz, *Sol. Energy Mater. Sol. Cells* **2017**, *173*, 96.
[65] F. Haase, C. Hollemann, S. Schaefer, A. Merkle, M. Rienaecker, J. Krügener, R. Brendel, R. Peibst, *Sol. Energy Mater. Sol. Cells* **2018**, *186*, 184.
[66] A. Cruz, D. Erfurt, P. Wagner, A. B. Morales-Vilches, F. Ruske, R. Schlatmann, B. Stannowski, *Sol. Energy Mater. Sol. Cells* **2022**, *236*, 111493.
[67] H. Lin, M. Yang, X. Ru, G. Wang, S. Yin, F. Peng, C. Hong, M. Qu, J. Lu, L. Fang, C. Han, P. Procel, O. Isabella, P. Gao, Z. Li, X. Xu, *Nat. Energy* **2023**, *8*, 789.
[68] R. Lin, J. Xu, M. Wei, Y. Wang, Z. Qin, Z. Liu, J. Wu, K. Xiao, B. Chen, S. M. Park, G. Chen, H. R. Atapattu, K. R. Graham, J. Xu, J. Zhu, L. Li, C. Zhang, E. H. Sargent, H. Tan, *Nature* **2022**, *603*, 73.
[69] T. Li, J. Xu, R. Lin, S. Teale, H. Li, Z. Liu, C. Duan, Q. Zhao, K. Xiao, P. Wu, B. Chen, S. Jiang, S. Xiong, H. Luo, S. Wan, L. Li, Q. Bao, Y. Tian, X. Gao, J. Xie, E. H. Sargent, H. Tan, *Nat. Energy* **2023**, *8*, 610.
[70] W. Chen, Y. Zhu, J. Xiu, G. Chen, H. Liang, S. Liu, H. Xue, E. Birgersson, J. W. Ho, X. Qin, J. Lin, R. Ma, T. Liu, Y. He,

A. M.–C. Ng, X. Guo, Z. He, H. Yan, A. B. Djurišić, Y. Hou, *Nat. Energy* **2022**, *7*, 229.
[71] M. Kim, J. Jeong, H. Lu, T. K. Lee, F. T. Eickemeyer, Y. Liu, I. W. Choi, S. J. Choi, Y. Jo, H.-B. Kim, S.–I. Mo, Y.–K. Kim, H. Lee, N. G. An, S. Cho, W. R. Tress, S. M. Zakeeruddin, A. Hagfeldt, J. Y. Kim, M. Grätzel, D. S. Kim, *Science* **2022**, *375*, 302.
[72] R. He, Z. Yi, Y. Luo, J. Luo, Q. Wei, H. Lai, H. Huang, B. Zou, G. Cui, W. Wang, C. Xiao, S. Ren, C. Chen, C. Wang, G. Xing, F. Fu, D. Zhao, *Adv. Sci.* **2022**, *9*, 2203210.
[73] R. He, W. Wang, Z. Yi, F. Lang, C. Chen, J. Luo, J. Zhu, J. Thiesbrummel, S. Shah, K. Wei, Y. Luo, C. Wang, H. Lai, H. Huang, J. Zhou, B. Zou, X. Yin, S. Ren, X. Hao, L. Wu, J. Zhang, M. Stolterfoht, F. Hu, W. Tang, D. Zhao, *Nature* **2023**, *618*, 80.
[74] H. Liu, J. Dong, P. Wang, B. Shi, Y. Zhao, X. Zhang, *Adv. Funct. Mater.* **2023**, *33*, 2303673.
[75] M. Wanlass, *US Patent 9,590,131 B2*, **2017**.
[76] B. M. Kayes, H. Nie, R. Twist, S. G. Spruytte, F. Reinhardt, I. C. Kizilyalli, G. S. Higashi, in *2011 37th IEEE Photovoltaic Specialists Conf.*, IEEE, Piscataway, NJ **2011**.
[77] D. Lackner, O. Höhn, R. Müller, P. Beutel, P. Schygulla, H. Hauser, F. Predan, G. Siefer, M. Schachtner, J. Schön, J. Benick, M. Hermle, F. Dimroth, *Sol. RRL* **2020**, *4*, 2000210.
[78] O. Almora, C. I. Cabrera, J. Garcia-Cerrillo, T. Kirchartz, U. Rau, C. J. Brabec, *Adv. Energy Mater.* **2021**, *11*, 2100022.
[79] E. Aydin, T. G. Allen, M. De Bastiani, L. Xu, J. Ávila, M. Salvador, E. Van Kerschaver, S. De Wolf, *Nat. Energy* **2020**, *5*, 851.
[80] H. Shen, J. Peng, D. Jacobs, N. Wu, J. Gong, Y. Wu, S. K. Karuturi, X. Fu, K. Weber, X. Xiao, T. P. White, K. Catchpolea, *Energy Environ. Sci.* **2018**, *11*, 394.
[81] M. Jošt, E. Köhnen, A. Al-Ashouri, T. Bertram, Š. Tomšič, A. Magomedov, E. Kasparavicius, T. Kodalle, B. Lipovšek, V. Getautis, R. Schlatmann, C. A. Kaufmann, S. Albrecht, M. Topicč, *ACS Energy Lett.* **2022**, *7*, 1298.

